World Academy of Science, Engineering and Technology
International Journal of Mechanical and Mechatronics Engineering
Vol:7, No:10, 2013

Numerical Investigation of Non-Newtonians Fluids Flows between Two Rotating Cylinders Using Lattice Boltzmann Method

S. Khali, R. Nebbali, K. Bouhadef

***Abstract*—**A numerical investigation is performed for non Newtonian fluids flow between two concentric cylinders. The D2Q9 lattice Boltzmann model developed from the Bhatangar-Gross-Krook (LBGK) approximation is used to obtain the flow field for fluids obeying to the power-law model. The inner and outer cylinders rotate in the same and the opposite direction while the end walls are maintained at rest. The combined effects of the Reynolds number (Re) of the inner and outer cylinders, the radius ratio (η) as well as the power-law index (n) on the flow characteristics are analyzed for an annular space of a finite aspect ratio (Γ). Two flow modes are obtained: a primary mode (laminar stable regime) and a secondary mode (laminar unstable regime). The so obtained flow structures are different from one mode to another. The transition critical Reynolds number Re_c from the primary to the secondary mode is analyzed for the co-courant and counter-courant flows. This critical value increases as n increases. The prediction of the swirling flow of non Newtonians fluids in axisymmetric geometries is shown in the present work.

***Keywords*—**Taylor-Couette flows, non Newtonian fluid, Lattice Boltzmann method.

I. Introduction

FLUIDS contained between two concentric cylinders rotating in the same and the opposite direction has been the subject of many experimental, analytical and numerical studies. This interest is motivated by the several industrial applications of this device such as journal bearings, purification of industrial wastewater and oil drilling. Taylor [1] conducted an experimental and theoretical investigation on the stability of a viscous flow in a small annular gap between two concentric cylinders with the inner one rotating. Diprima [2] found that the flow is relatively stable when the outer cylinder is rotating. H.-S. Dou et al. [3] proposed a method for calculating the energy loss distribution in the Taylor–Couette flow between concentric rotating cylinders. The principle and the detailed derivation for the calculation are given for a single cylinder rotation of either the inner or outer cylinder. They considered the cases of rotations in the same direction and the opposite direction.

Benjamin [4] gave a qualitative description of the phenomenon of bifurcation and morphogenesis of the flow structure in the annular space with an aspect ratio of about 1. The experimental results were presented for the location of bifurcation critical points and flow profiles.

Researchers have dedicated many studies to Newtonian fluids despite, in practical applications the fluids drift away from the Newtonian idealized model. Thus, to take into account of this aspect more and more studies are devoted to non-Newtonian fluids. There was a considerable interest to non Newtonian Taylor-Couette instability .Sinevic et al. [5] determined the onset of Taylor vortices by measuring the torque exerted by a non-Newtonian fluid on the rotating inner cylinder.

Recently, measurements of velocity fields for the Taylor Couette flow have been performed by Wereley and Lueptow [6] using particle image velocimetry (PIV), the authors showed a rich variety of flow regimes that can occur for cylindrical Couette flow with an imposed axial flow, depending upon Taylor number and Reynolds number. Lockett et al. [7] simulated the transition flow using a finite element method. The authors found that the stabilizing or destabilizing effect induced by the shear-thinning behavior depends on the radius ratio. Escudier et al. [8] investigated the flow structure in Taylor-Couette geometry with a large radius ratio. Axial and tangential velocity measurements were made using a laser Doppler anemometer.

During the last years, the LBM have received a considerable attention by fluid dynamic researchers. It has been shown that this method is an attractive alternative to classical numerical schemes due to its inherent advantages such as its simple implementation, high parallelizability and great convenience of handling complicated geometries. Khali et al. [9] investigated the instability of the Taylor-Couette flow of the Newtonian and non-Newtonian fluids (pseudoplastic and dilatant fluids) for cases of finite aspect ratios using lattice Boltzmann method (LBM). They showed that the critical Reynolds number Re_c for the passage from the first mode of the Couette flow (CF) to the secondary mode Taylor vortex flow regime (TVF) exhibits the lowest value for the pseudoplastic fluids and the highest value for the dilatant fluids.

The purpose of this work is to investigate the stability of the Taylor Couette flow of Newtonian and non Newtonian fluids with finite aspect ratios using the Lattice Boltzmann Method (LBM). The two cylinders can rotate either in the same or in the opposite direction while the end caps are maintained at rest. The model proposed by Huang et al. [10] for the axisymmetric LMB has been adopted. The velocity and stream function distributions along the annular duct are compared

S. Khali, R. Nebbali, and K. Bouhadef are with the Faculty of Mechanical and Process Engineering (FGMGP), Laboratory of Multiphase Transport and Porous Media (LTPMP) B.P.32, El Alia Bab Ezzouar 16111, Algiers, Algeria (e-mail: khalisamir2005@ yahoo.fr, rnebbali@ usthb.dz).

with analytical and numerical solutions. The combined effects of the Reynolds numbers and the power-law index of the non-Newtonians fluids on the flow characteristics are analyzed.

II. Lattice Boltzmann Method

The standard LBM was first developed for Cartesian coordinates system. To handle axisymmetric problems with this method, without using 3D lattices system, a source term is introduced in the original LB equation as it was done by Halliday et al. [11].

The three-dimensional axisymmetric Navier-Stokes equations are written in a pseudo Cartesian form with making the following replacement:

$$(r,z) \rightarrow (x,y) \text{ and } (u_r,u_z,u_\theta) \rightarrow (u,v,w)$$
$$\partial_j u_j = -u_r/r \quad (1)$$

$$\rho[\partial_t u_i + \partial_j(u_i u_j)] = -\partial_i p + \mu\partial_j^2 u_i + \mu u_i u_r/r - \mu u_i/r^2\,\delta_{ir} \quad (2)$$

Bearing in mind that, in the standard LB method the recovered macroscopic momentum equation is written like:

$$\rho[\partial_t u_i + \partial_j(u_i u_j)] = -\partial_i p + \partial_j[\mu(\partial_i u_j + \partial_j u_i)] \quad (3)$$

Therefore we need to rewrite (2) as:

$$\rho[\partial_t u_i + \partial_j(u_i u_j)] = -\partial_i p + \partial_j[\mu(\partial_i u_j + \partial_j u_i)] + \mu(\partial_r u_i + \partial_i u_r)/r - \rho u_i u_r/r - 2\,\mu u_i \delta_{ir}/r^2 \quad (4)$$

Compared with the form in the (x, y) plane, the two terms in the right hand side of the above equation can be considered as body forces. Now we follow the idea of Halliday et al. [11] and derive an LBE which recovers (1) and (2) from an incompressible D2Q9 model. The discrete velocities of this model are as follow:

$$\begin{cases} (0,0) & i = 0 \\ c\left(\cos\left[\frac{(i-1)\pi}{2}\right], \sin\left[\frac{(i-1)\pi}{2}\right]\right) & i = 1,2,3,4 \\ c\sqrt{2}\left(\cos\left[\frac{(i-5)\pi}{2}+\frac{\pi}{4}\right], \sin\left[\frac{(i-5)\pi}{2}+\frac{\pi}{4}\right]\right) & i = 5,6,7,8 \end{cases} \quad (5)$$

where: $c = \delta x/\delta t$

Note that δx and δt are, respectively, the lattice spacing and the time step. Both are set to unity. The two-dimensional LBE describing 2D flow in (x, r) pseudo-Cartesian coordinates is constructed as follow:

$$f_i(x + ce_{iz}\delta_t, r + ce_{ir}\delta_t, t + \delta_t) = f_i(x,r,t) + \frac{1}{\tau}\left[f_i^{eq}(x,r,t) - f_i(x,r,t)\right] + S_i(x,r,t) \quad (6)$$

where τ is the relaxation time, f_i is the density distribution function along the i direction, $e_i(e_{ir}, e_{iz})$ is the particle velocity in the i direction, f_i^{eq} is the corresponding equilibrium state distribution function, which can be written as:

$$f_i^{eq}(x,r,t) = \omega_i p/c_s^2 + \rho\omega_i[e_i u/c_s^2 + (e_i u)^2/2c_s^4 - u^2/2c_s^2] \quad (7)$$

In the above equation $c_s = c/\sqrt{3}$ is the sound speed, p is the pressure and $\rho$is the fluid density. The constant factors ω_i differ from a model to another (in the D2Q9, ω0 =4/9, ω_i=1/9 for i=1, 2, 3, 4 and ω_i=1/36 for i=5, 6, 7, 8).

The relaxation time τ and the fluid viscosity ν are linked as follows:

$$\nu = (2\tau - 1)\,\delta_x/6 \quad (8)$$

To avoid numerical instabilities and for a positive physical viscosity, τ is generally, taken greater than 0.5 [8]

The term S_i (z, r, t) in (6) is defined as a function of a spatial (space) and velocity. It can be expressed as:

$$S_i = \delta_t S_i^{(1)} + \delta_t^2 S_i^{(2)} \quad (9)$$

where $S_i^{(1)}$and $S_i^{(2)}$respectively, represent the zeroth and first order gradients of the macroscopic variables ρ, u. By performing a Chapman- Enskog expansion, we obtain the following development:

$$S_i^{(1)} = -\omega_i \rho u_r/r \quad (10)$$

$$\begin{aligned} S_i^{(2)} = {} & \omega_i[\partial_r(p/\rho) + \partial_z(u_z u_r) + \partial_r(u_r u_r)]/2r \\ & + 3\omega_i\nu[\partial_r u_z e_{iz} + \partial_r u_r e_{ir} - u_r e_{ir}/r]/r \\ & - 3\omega_i u_r(u_z e_{iz} + u_r e_{ir})/r \\ & -\omega_i(1-\tau)((\partial_z u_r/r)e_{iz} - u_r e_{ir}/r^2) \\ & +\omega_i(1-\tau)(\partial_r u_r/r)e_{ir} + 3\omega_i(u_\theta^2 e_{ir}/r) \end{aligned} \quad (11)$$

For the velocity derivations in (11), the terms $\partial_r u_z$, $\partial_z u_r$, $\partial_z u_z$ and $\partial_r u_r$can all be obtained through (12) with replacing $\alpha = z, \beta = r, \alpha = \beta = z$ and $\alpha = \beta = r$ respectively:

$$(\partial_\beta u_\alpha + \partial_\alpha u_\beta) - 1/\rho\nu\,(1 - 1/2\tau)\,\sum_{i=0}^{8} f_i^{ne}\, e_{i\alpha} e_{i\beta} + O(\varepsilon^2) \quad (12)$$

Only the remaining term $\partial_z u_r$is obtained by using a second order finite difference scheme. It is given by:

$$(\partial_z u_r)_{i,j} = \left((u_r)_{i,j+1} - (u_r)_{i,j-1}\right)/2\delta_x \quad (13)$$

In the streaming step, the distribution function new value obtained from (6) would propagate to adjacent eight lattices. That procedure can be represented as follows:

$$f_i(x + ce_{iz}\delta_t, r + ce_{ir}\delta_t, t + \delta_t) = f_{i\_new}(z,r,t) \quad (14)$$

The basic hydrodynamic quantities, such as density ρ and velocity u, are obtained through moment summations in the velocity space:

$$\rho(x,t) = \sum_i f_i(x,t), \quad \rho u(x,t) = \sum_i e_i f_i(x,t) \quad (15)$$

III. Physical Problem

We consider the flow of non-Newtonian fluids between two finite concentric cylinders with inner radius r_i and outer radius r_e. The cylinders rotate independently with inner and outer angular velocities Ω_i and Ω_e. The Reynolds numbers based on the azimuthal velocities and the annulus gap are defined as $Re_i= (\Omega_i\ r_i).d/\upsilon$ and $Re_e= (\Omega_e\ r_e)d/\upsilon$ for respectively the inner and the outer cylinder. Where $d=(r_e-r_i)$ is the annulus gap and υ is the fluid viscosity.

The annulus is characterized by the radius ratio $\eta=r_i/r_e$ and the aspect ratio $\Gamma=H/(r_i-r_e)$, where H is the height of the annulus.

In order to formulate the problem, it is assumed that the flow is incompressible and axisymmetric. The commonly used power-law model, for non-Newtonian fluids, is adopted. The viscosity varies with the local shear rate $\dot{\gamma}$ in the form:

$$\mu = \mu_a|\dot{\gamma}|^{n-1} \tag{16}$$

where n is the power-law exponent and μ_a is the apparent viscosity.

Note that when n=1, the fluid corresponds to the Newtonian fluid, and μ_a is the Newtonian fluid viscosity. For fluids with n>1, the effective viscosity increases with the shear rate, and are called 'shear-thickening' or 'dilatants' fluids. While for 0<n<1, the effective viscosity decreases with the shear rate, and in this case the fluids are called 'shear-thinning' or 'pseudoplastic' fluids.

Regarding the relatively low angular velocities considered in the present study the shear rate $\dot{\gamma}$ is given by [9]

$$\dot{\gamma} = 2\left[\left(\frac{\partial u_r}{\partial r}\right)^2 + \left(\frac{u_r}{2}\right)^2 + \left(\frac{\partial u_z}{\partial z}\right)^2\right] + \left[r\frac{\partial}{\partial r}\left(\frac{u_\theta}{r}\right)\right]^2 + \left(\frac{\partial u_\theta}{\partial z}\right)^2 + \left(\frac{\partial u_z}{\partial r} + \frac{\partial u_r}{\partial z}\right)^2 \tag{17}$$

Coupling (8) and (16), we obtain a shear-dependent relaxation time at each node in the lattice Boltzmann evolution.

The azimuthal velocity is obtained through the following equation by using the first-order forward difference scheme in time and the second-order central difference scheme in space [10]:

$$u_\theta^{n+1} = \delta_t\left[-\left(u_z\frac{\partial u_\theta}{\partial z} + u_r\frac{\partial u_\theta}{\partial r}\right) + \nu\left(\frac{\partial^2 u_\theta}{\partial z^2} + \frac{\partial^2 u_\theta}{\partial r^2}\right) + \frac{\nu}{r}\left(\frac{\partial u_\theta}{\partial r} - \frac{u_\theta}{r}\right) - \frac{u_r u_\theta}{r}\right]^n - u_\theta^n \tag{18}$$

Modeling of the boundary conditions is very important in numerical modeling because they affect the overall accuracy and stability of the numerical scheme. Two kinds of boundary conditions are used to describe the non slip condition in the present work. On the inner and the outer cylinders the specular reflection is adopted while on the two end plates, the bounce-back condition is applied. This type of conditions supposes that the post-collision distribution function at the solid nodes with a velocity $-e_i$ is set equal to the post-collision distribution function at the fluid nodes with a velocity e_i.

TABLE I
Grid Independency Tests

Mesh	Ψmax (Re=85)	Ψmax(Re=100)
20×76	$4.800\ 10^{-2}$	$5.465\ 10^{-2}$
30×114	$4.876\ 10^{-2}$	$5.555\ 10^{-2}$
40×152	$4.908\ 10^{-2}$	$5.594\ 10^{-2}$
50×190	$4.924\ 10^{-2}$	$5.623\ 10^{-2}$
60×228	$4.936\ 10^{-2}$	$5.636\ 10^{-2}$
Error (max)	%1.58	%1.64

IV. Results and Interpretations

A. Mesh Sensitivity

The required number of lattices is obtained by a grid sensitivity analysis in order to insure accurate results. Table I summarizes this analysis for the case of γ=0.5, Γ=3.8, Re=85 and 100.

To stop the computational process, the convergence criterion below reported in [10] has been used:

$$\sum_{i,j}\frac{\left\|\sqrt{\left(u_z(x_i,r_j,t+\delta_t)-u_z(x_i,r_j,t)\right)^2+\left(u_r(x_i,r_j,t+\delta_t)-u_r(x_i,r_j,t)\right)^2}\right\|}{\left\|\sqrt{u_z(x_i,r_j,t+\delta_t)^2+u_r(x_i,r_j,t+\delta_t)^2}\right\|}$$

where i, j are the lattice nodes indices.

TABLE II
Comparison of Ψmax against Literature Results

Re	Present work	Huang et al. [9]	Niu et al. [13]	ε max
85	4.903×10-2	4.810×10-2	4.859×10-2	1.82 %
100	5.553×10-2	5.501×10-2	5.580×10-2	0.93 %
150	6.361×10-2	6.427×10-2	6.387×10-2	1.25 %

B. Validation of the Computational Code

To verify the accuracy of our LBM code predicting the Taylor Couette flow of non-Newtonians fluids, some validation tests were performed. First, the efficiency of our results was checked against results of Huang et al. [10] and Niu [12]. The case of a Taylor–Couette flow with an aspect ratio of 3.8 with a Newtonian fluid (n=1), for Re=85, 100 and 150 using a mesh of 20×76 lattices was successfully simulated and the maximum deviation of Ψ_{max} does not exceed 1.82% as shown in Table II.

For low Reynolds numbers, the present axisymmetric Lattice Boltzmann code successfully recovers the analytical profile of the azimuthal velocity [13] as it is shown in Fig. 1.

$$u_\theta(r) = \frac{r}{r_i}\left[1 - \left(\frac{1}{r_e^{2/n}} - \frac{1}{r_i^{2/n}}\right)^{-1}\left(\frac{1}{r^{2/n}} - \frac{1}{r_i^{2/n}}\right)\right] \tag{19}$$

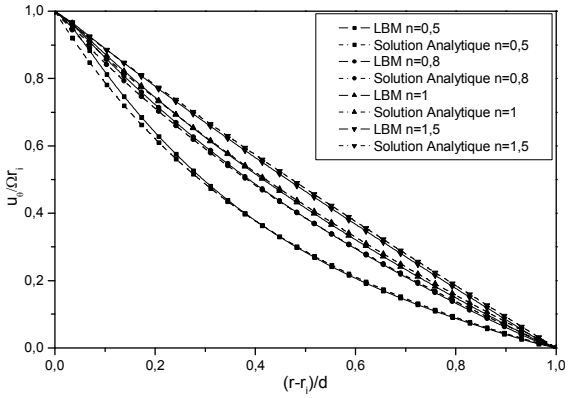

Fig. 1 Comparison of the azimuthal velocity with analytical solution. For γ=0.5, Γ=3.8

Due to the numerous parameters controlling the flow configuration, all the computations have been performed by setting fixed the aspect ratio to 6, the mesh size to 20×120 and the radius ratio to 0.5. For the non Newtonians fluids flows the exponent *n* was chosen in the range between 0.5 and 1.5 while both Reynolds number were varied from 20 to 150.

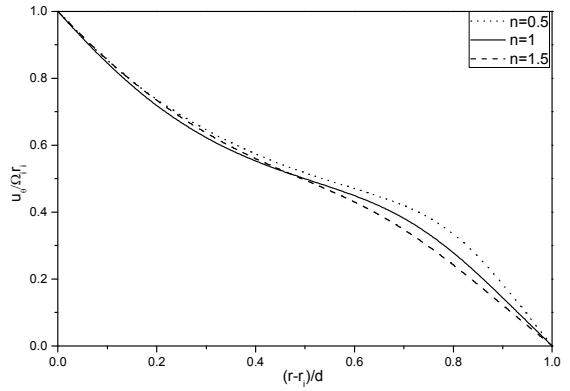

Fig. 2 Variations of the Azimuthal velocity profiles for different fluids for γ=0.5 and Γ=6 (Re_i=100 and Re_e=0)

Fig. 2 illustrates the dimensionless azimuthal velocity variations versus the radial position for different values of the power-law index *n*. It shows that the velocity profile decays gradually along the radial position for the considered fluids. We note that the azimuthal velocity exhibits two distinct behaviours as function of *n* in the annulus space. For approximately 0.5<r≤1, the augmentation of *n* decreases the velocity modulus, while, when r < 0.5, *n* no longer has any effect on the velocity profile. Moreover, the azimuthal velocity gradients are more important for the pseudoplastic fluids than the dilatants fluids.

To show the flow structures occurring in the Taylor–Couette apparatus with a rotating outer cylinder. The flow states between counter and co-rotating cylinders is observed for the selected range of Reynolds numbers. The flow structures transitions were obtained by fixing the outer cylinder Reynolds number Re_e first and slowly increasing Re_i.

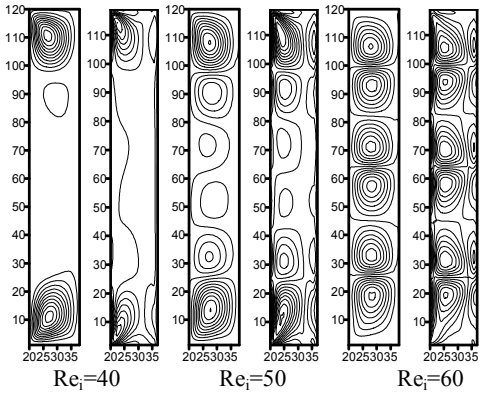

(a)

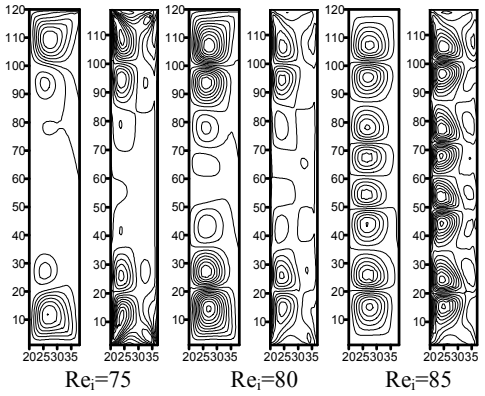

(b)

Fig. 3 Contours of streamlines (left) and vorticity (right) fields for n =0.5 and Γ=6. a-Re=-10, b- Re=-40

The flow structure of the pseudoplastic fluid with counter-rotating cylinders is shown in the Fig. 3. We note that the increasing of the Reynolds number in the opposite direction delay the first instability appearance in the annulus and the number of cells increase from 6-cells to 8-cells as shown in Fig. 3.

For the dilatant fluid, we note, in Fig. 4, that the increase of the outer cylinder Reynolds number has a weak effect on the transition to the Taylor vortex flow (TVF) compared with the pseudoplastic fluid. This can be explained by the increase of the fluid viscosity due to higher power law index, which lead to a stabilising effect on the flow structures.

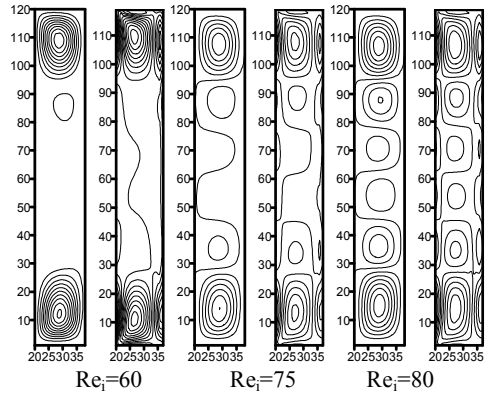

(a)

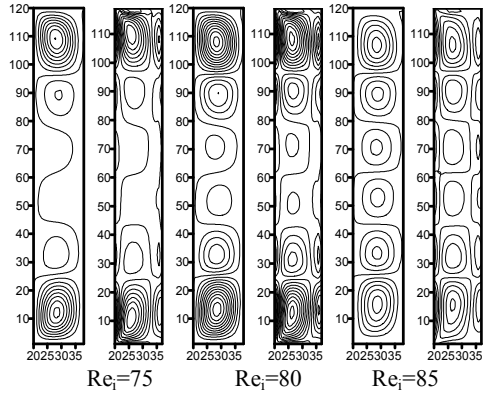

(b)

Fig. 4 Contours of streamlines (left) and vorticity (right) fields for n =1.5 and Γ=6. a-Re=-10, b- Re=-40

The co-rotating effect on the transition from the Couette flow to the Taylor vortex flow is discussed in this section. For the pseudoplastic fluid, the increase of the outer cylinder Reynolds number decrease the number of the cells in the annulus from N=4 to N=2 as illustrated in Fig. 5. We note that the number of cells does not change in the duct for Re$_e$=40. This phenomenon can be explained by the great end caps influence. The two cells attached to the ends above the Taylor vortices reach such importance that they prevent the development of Taylor vortices with opposite rotation, even for high Reynolds numbers.

The flow structure for the dilatants fluids is given in Fig. 6. One can note that the increase of the inner Reynolds number (Re$_i$) slow down the transition to the TVF regime and the flow is more stable for the co-rotating case compared with the counter-rotating case. We also note that the impact of the external cylinder rotation diminishes.

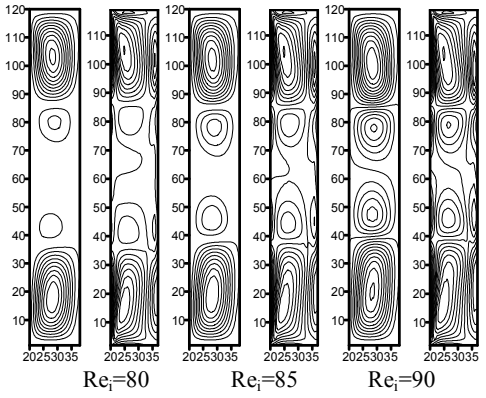

(a)

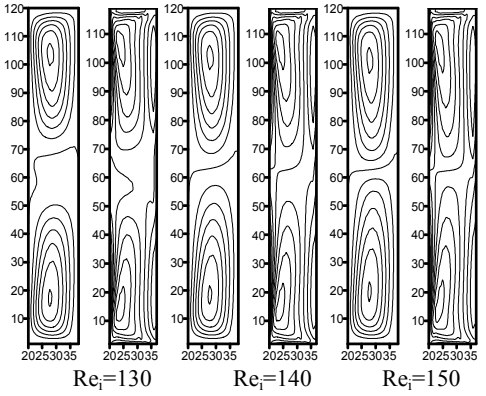

(b)

Fig. 5 Contours of streamlines (left) and vorticity (right) fields for n =0.5 and Γ=6. a-Re=10, b- Re=40

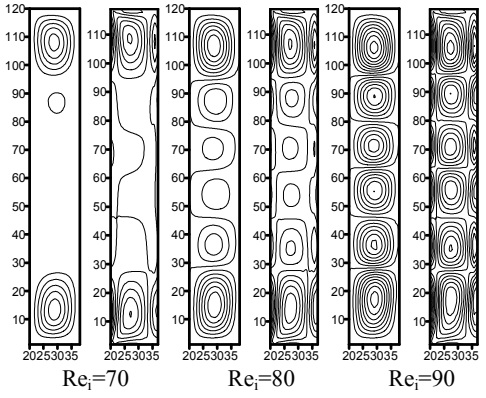

(a)

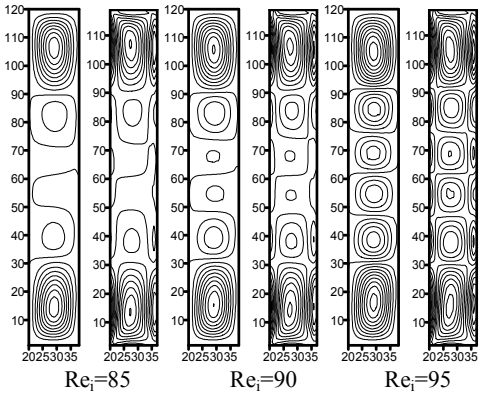

(b)

Fig. 6 Contours of streamlines (left) and vorticity (right) fields for n =1.5 and Γ=6. (a) Re=10, (b) Re=40

Fig. 7 shows the variation of the azimuthal velocity for different outer Reynolds number while the inner Reynolds number is fixed to Re_i=30. We note that for counter-courant and co-courant flow, the variations of u_z close to the two fixed end caps are characterized by important slopes and exhibiting the highest and lowest values. This indicates the presence of two vortexes attached in the two fixed extremities. For the co-courant flow (Fig. 7 (a)), as Re_e increases, the extremum values decrease lowering the intensity of the attached eddies to the end caps, and the u_z forms a straight inclined which indicates that the two ends vortices approach in the middle of the pipe. For the counter-courant case (Fig. 7 (b)), the increase of Re_e in opposite direction implies a variation of the azimuthal velocity near the fixed ends and vortex intensities and the two ends vortex recede.

The evolution of the azimuthal velocity in the radial direction is shown in Fig. 8. For a fixed position, the increase of the outer Reynolds number led the increase of the azimuthal velocity in the annulus and it is more significant for the counter-rotating case close to 0.5 in the radial direction. The variation of the azimuthal velocity due to the outer Reynolds number is more expressed near the outer cylinder zone.

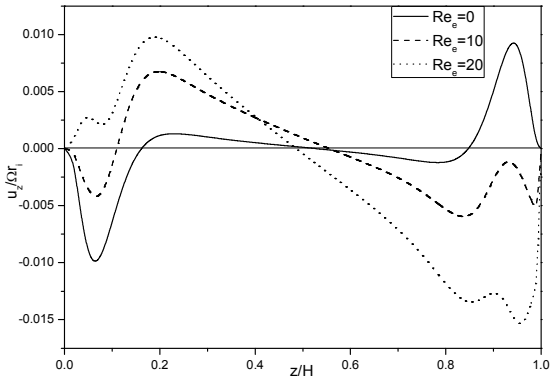

(a)

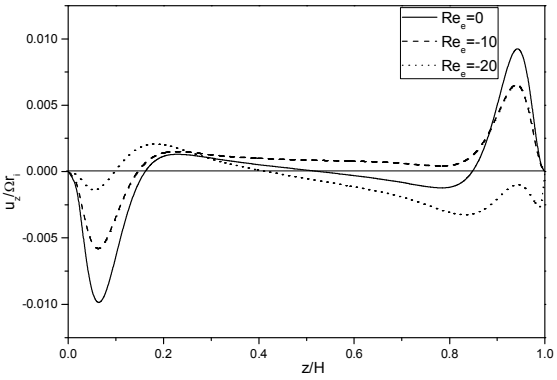

(b)

Fig. 7 Variations of the azimuthal velocity arofiles for different Reynolds numbers of the outer cylinder for Rei =30, η=0.5 and Γ=6

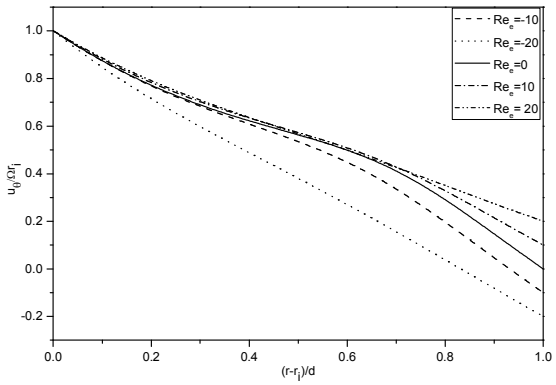

Fig. 8 Variations of the Azimuthal velocity Profiles for different Reynolds numbers at η=0.5 and Γ=6

The effect of the rotation of the outer cylinder on the apparition of the first instability in the annuli is shown in Fig. 9. We note that for all fluids, the rotation of the outer cylinder with co-courant or counter-courant make a variation of the critical Reynolds number for the transition from the Couette flow (CF) regime to the Taylor vortex flow (TVF) regime and Re_{ic} increase with the power law index n. Moreover, there is a range of Re_e (negative value) for which the critical Reynolds number decreases and this interval augments as n decreases.

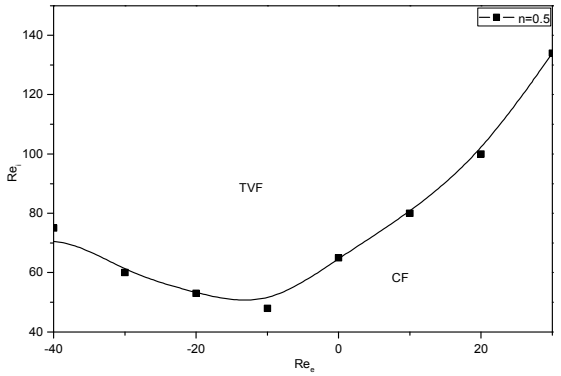

(a)

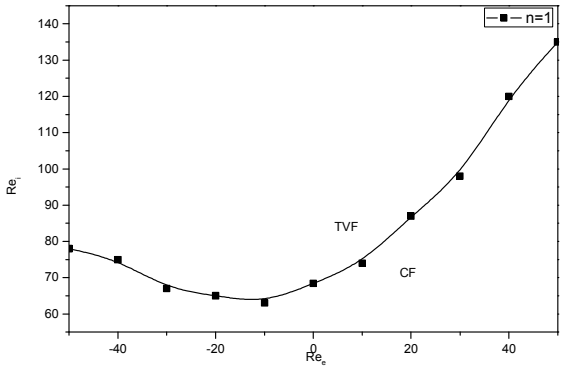

(b)

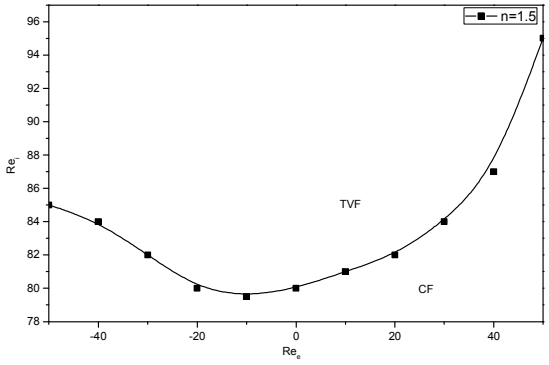

(c)

Fig. 9 Critical condition for the primary instability for counter and co-rotating cylinders with η=0.5, Recorded is the inner cylinder Reynolds number Re_i versus Re_e, the outer cylinder one

V. Conclusion

A numerical investigation has been developed for the flow of non Newtonians fluids between two concentric cylinders using the lattice Boltzmann method D2Q9 model. Flow states between counter and co-rotating cylinders were observed for the selected range of Reynolds numbers and the transitions regimes were located by first fixing Re_e and then slowly increasing Re_i while the end caps are kept at rest. For low Reynolds numbers, the present axisymmetric Lattice Boltzmann code has been validated against an analytical expression of azimuthal velocity and available literature results for the Taylor Couette flow. The effect on the flow pattern of several parameters such as the Reynolds numbers and the power-law index has been analyzed. For Taylor Couette flow with counter-rotation ($\Omega_1\Omega_2<0$) and a fixed Re_e, the increasing of the Reynolds number in the opposite direction delay the appearance of the first instability in the annulus. Moreover, the number of cells increases from 6-cells to 8-cells for pseudoplastic fluids and does not have a large effect on the transition to the Taylor vortex flow for dilatant fluids. For the case of Taylor Couette flow with co-rotating cylinders Ω_1 $\Omega_2>0$, the increase of the outer cylinder Reynolds number decreases the number of the cells in the annulus. For the dilatant fluid, the increase of the inner Reynolds number (Re_i) slow down the transition to the TVF regime and the flow is more stable for the co-rotating case.

References

[1] G. I. Taylor, "Stability of viscous liquid contained between two rotating cylinders", Phil. Trans. R. Soc. London, A223:289–343, (1923).

[2] R. C. Diprima and P.M. Eagles, "The effect of radius ratio on the stability of Couette flow and Taylor vortex flow", Phys. Fluids, 27, 2403-2411, (1984).

[3] H. -S. Dou, B. C. Khoo, K. S. Yeo, "Energy loss distribution in the plane Couette flow and the Taylor–Couetteflow between concentric rotating cylinders", Int. J. of Thermal Sciences 46, 262–275,(2007).

[4] T. B. Benjamin, "Bifurcation phenomena in steady flow of a viscous fluid Part I and II", Proc. R. Soc. London, Ser. A 359, 1 (1978).

[5] V. Sinevic, R. Kuboi, and A. W. Nienow, "Power numbers, Taylor numbers and Taylor vortices in viscous Newtonian and non-Newtonian fluids", Chemical. Engineering. Science, 41:2915–2923, (1986).

[6] S. T. Wereley, and R.M. Lueptow, "Spatio-temporal character of non-wavy and wavy Taylor-Couette flow", J. Fluid Mech. 364, 59–80, (1998).

[7] T. J. Lockett, S. M. Richardson, and W. J. Worraker, "The stability of inelastic non-Newtonian fluids in Couette flow between concentric cylinders: a finite element study", J. Non-Newtonian Fluid Mech. 43:165–177, (1992).

[8] M. P. Escudier, I. W. Gouldson, and D. M. Jones, "Taylor vortices in Newtonian and shear-thinning liquids", Proceedings - Royal Society of London, A 449 (1935):155–176, (1995).

[9] S. Khali, R. Nebbali, D. E. Ameziani, and K. Bouhadef, "Numerical investigation of non-Newtonian fluids in annular ducts with finite aspect ratio using lattice Boltzmann method", Physical Review E 87, 053002 (2013).

[10] H. Huang, T. S. Lee, and C. Shu, "Hybrid lattice Boltzmann finite-difference simulation of axisymmetric swirling and rotating flows", Int. J. Num. Meth. Heat & Fluid Flow, Vol. 17, p. 587-607, (2007).

[11] I. Halliday, and L. A. Hammond, "Care, Enhanced closure scheme for lattice Boltzmann equation hydrodynamics", J. Phys. A: Math. Gen, Vol. 35, p. 157–166, (2002).

[12] X. D. Niu, C. Y. Shu, and T. Chew, "An axisymmetric lattice Boltzmann model for simulation of Taylor-Couette flows between two concentric cylinders", Int. J. of Modern Physics, Vol. 14, No 6, p. 785–796, (2003).

[13] A. Brahim, C. Lemaitre, C. Nouar, and N. Ait-Moussa, "Revisiting the stability of circular Couette flow of shear-thinning fluids", J. Non-Newtonian Fluid Mech. 183-184, 37 (2012).